Ventilation-Synchronous Magnetic Resonance Microscopy of Pulmonary Structure and Ventilation in Mice

Ben T. Chen,[1] Alexander T. Yordanov,[2] and G. Allan Johnson[1]

Increasing use of transgenic animal models for pulmonary disease has raised the need for methods to assess pulmonary structure and function in a physiologically stable mouse. We report here an integrated protocol using magnetic resonance microscopy with gadolinium (Gd)-labeled starburst dendrimer (G6–1B4M-Gd, MW = 192 ± 1 kDa, R_h = 5.50 ± 0.04 nm) and hyperpolarized ^{3}helium (^{3}He) gas to acquire images that demonstrate pulmonary vasculature and ventilated airways in live mice (n = 9). Registered three-dimensional images of ^{1}H and ^{3}He were acquired during breath-hold at 2.0 T using radial acquisition (total acquisition time of 38 and 25 min, respectively). The macromolecular Gd-labeled dendrimer (a half-life of ~80 min) increased the signal-to-noise by 81 ± 30% in the left ventricle, 43 ± 22% in the lung periphery, and −4 ± 5% in the chest wall, thus increasing the contrast of these structures relative to the less vascular surrounding tissues. A constant-flow ventilator was developed for the mouse to deliver varied gas mixtures of O_2 and N_2 (or ^{3}He) during imaging. To avoid hypoxemia, instrumental dead space was minimized and corrections were made to tidal volume lost due to gas compression. The stability of the physiologic support was assessed by the lack of spontaneous breathing and maintenance of a constant heart rate. We were able to stabilize the mouse for >8 hr using ventilation of 105 breath/min and ~0.2 mL/breath. The feasibility of acquiring both pulmonary vasculature and ventilated airways was demonstrated in the mouse lung with in-plane spatial resolution of 70 × 70 μm^2 and slice thickness of 800 μm. Magn Reson Med 53:69–75, 2005. © 2004 Wiley-Liss, Inc.

Key words: ventilation-synchronous; lung imaging; dendrimer; hyperpolarized helium; coregistered imaging

Transgenic and knockout mice have become critical models for studying lung diseases, such as emphysema (1), fibrosis (2), and asthma (3,4). Magnetic resonance microscopy (MRM) presents a particularly appealing method for both structural and ventilatory phenotyping in these models, but the technical challenges in performing such studies in the mouse lung are formidable. Specifically, ventilation-gated synchronous scanning is required to produce high-resolution magnetic resonance (MR) lung images of a live animal without blurring. To date, such MR imaging studies that have been performed in rodents have generally been performed in rats (5–10) with only limited recent application in the mouse (11). The mouse, at 25 g, is at least 10 times smaller than the rat with a heart rate nearly 2-times greater than that of the rat, which poses challenges in both life support and physiologic measurement. Mechanical ventilation generally requires intubation of the animal (12). As inhalation and exhalation share the common conducting (nonrespiratory) passage, instrumental dead space (the volume of the exhaust air re-entering the lung) is inevitable in the respiratory system. Since the tidal volume (TV) used to maintain a mouse is 200–300 μL, the endotracheal tube commonly used for intubation can significantly increase the portion of exhaust air in the TV, resulting in hypoxemia or death. In addition, because of gas compression, precise delivery of a small quantity of air into a high-impedance mouse lung is technically challenging. Thus, current methods for physiologic support of rats are not sufficient for use in mice.

In vivo lung imaging in small animals using MR has been difficult due to low spin density and susceptibility variations within air/tissue interfaces, as well as the cardiac and breathing motions in the animal. To address these problems, various scanning strategies have been developed for ^{1}H imaging of rat lung (6,9,13). Recent development of a hyperpolarized (HP) ^{3}He imaging technique has produced two- and three-dimensional (2D, 3D) functional lung imaging (9,14) and a quantitative measurement to assess regional ventilation distribution (15–17). A combination of the traditional ^{1}H imaging and HP ^{3}He imaging can provide a noninvasive assessment of structural and ventilatory information of the lung (8,9,17). But all of these studies have been performed in rats. Development of the physiologic support, the integration of HP ^{3}He, the development of a dual frequency (mouse) radiofrequency coil, the use of macromolecular contrast agents to highlight pulmonary vasculature, and the use of anisotropic 3D projection encoding methods with explicit attention to the unique size and physiology of the mouse are the focus of this work.

METHODS

Determination of Tidal Volume

By weight, a mouse (~25 g) requires only 1/10 of the ventilation needed for a rat (~250 g). As the TV gets smaller, it becomes increasingly difficult to provide adequate ventilation for mice because the dead space becomes a larger fraction of the TV. In addition, as the TV becomes smaller, compression of the gas becomes a much more significant problem than it is with rats. Both of these

[1]Center for In Vivo Microscopy, Duke University Medical Center, Durham, North Carolina.

[2]Department of Radiology, Duke University Medical Center, Durham, North Carolina.

Grant sponsor: NCRR/NCI National Resource; Grant number: P41 RR05959/R24 CA 92656; Grant sponsor: NIH/NHLBI; Grant number: R01 HL55348.

Correspondence to: G. Allan Johnson, c/o Sally Zimney, Center for In Vivo Microscopy, Box 3302, Duke University Medical Center, Durham, NC 27710. E-mail: sally.zimney@duke.edu

Received 27 April 2004; revised 29 July 2004; accepted 11 August 2004.

DOI 10.1002/mrm.20307

Published online in Wiley InterScience (www.interscience.wiley.com).

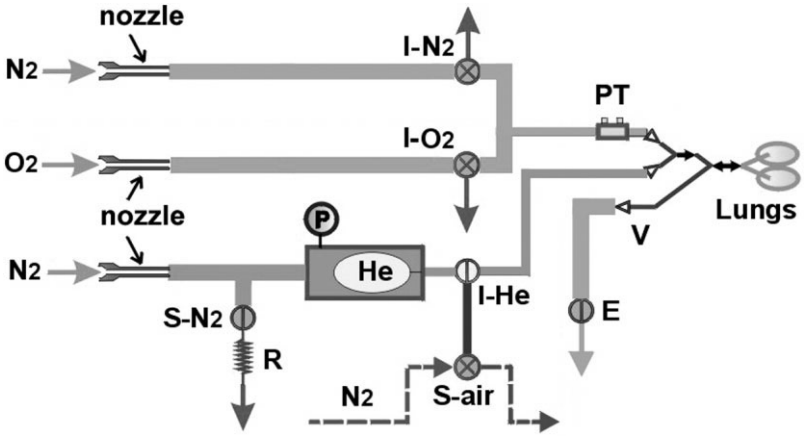

FIG. 1. Schematic of the ventilator showing the normal mode of ventilation and operation with ^{3}He. The nitrogen inlet (I-N_2), oxygen inlet (I-O_2) and exhalation valves (E) are solenoid valves to control gas flow to form a breathing cycle. The nitrogen supply valve (S-N_2) and an adjustable flow restrictor (R) regulate the N_2 gas into the Plexiglas chamber, which drives the hyperpolarized ^{3}He gas in a collapsible plastic bag into the lung. A pneumatic valve (I-He) controlled by the supply air (S-air) valve is used to regulate the HP ^{3}He gas. A pneumotachometer (PT) is placed in the inspiratory conduit for the normal mode to measure the airflow rate and air pressure. To prevent backflow, one-way valves (V) are used in the inspiratory and expiratory conduits.

factors can reduce the effectiveness and accuracy of mechanical ventilation. To overcome these problems, a constant flow ventilator developed previously for rats (17) was modified for mice. Figure 1 shows a schematic of the modified ventilator. Constant flow ventilation was achieved by accelerating the pressurized gas via a very high-resistance nozzle (46,800 Lohm) to above the sonic speed. Under this critical condition, the gas flow was independent of dynamic changes of lung resistance and was proportional to the applied positive gas pressure. However, mice have higher pulmonary impedance (>10 times) than rats (18). With the higher impedance and the smaller TV, the actual volume of gas delivered to the lung is much less than the desired TV due to compression of the gas in the inspiratory line. Due to the high magnetic field (2 T), solenoid valves and pressure transducers used in the ventilator must be kept at a distance (~4 ft) from the mouse (Fig. 1). This resulted in a larger air volume in the inspiratory conduit and the pressure-sensed lines. Such a shortcoming magnified the problem of gas compression in the system. To estimate the actual TV, the gas compression within the ventilation system was characterized by

$$V_{\text{meas}} = V_t + V_c \text{ and } V_c = (P + C)/E,$$

where V_{meas} is the TV measured by a pneumotachometer (Series 8431B and Model RSS100HR, Hans Rudolph, Kansas City, MO), V_t is the actual TV, V_c is the gas volume not reaching the lung due to gas compression, P is the pressure measured in the pneumotachometer, C is a constant, and E is the compression index (cm-H_2O/mL) of the ventilation system. The V_c was measured at 105 breath/min by blocking the inspiratory vent at various inspired gas flow rates (19). Linear regression was applied (V_c versus. P) to determine the compression index. To verify the TV, a spirometer was used (Fig. 2). The TV corrected by compression index was verified with the spirometer at the applied pressure of 4 cm-H_2O (Fig. 2, water level b).

Mechanical Ventilation

Ventilation consisted of a positive-pressure forced inhalation and a passive exhalation. A single respiratory cycle is characterized by the inhalation period (I) and the period for exhalation (E). Lung images were acquired during a period of breath-hold, which was considered part of the inhalation period. To ensure the completion of exhalation, the animal was normally ventilated with an inhalation-to-exhalation ratio of 1/2. To provide a longer imaging window, the mouse was ventilated using a high inhalation-to-exhalation ratio (I = 229 msec, E = 343 msec, I/E = 2/3). Figure 3 shows the "Y" endotracheal tube (ET) consisting of separate inspiratory and expiratory channels used to minimize the dead space. This device allows adequate ventilation for a 25-g mouse using TV of 0.2 mL at 105 breath/min. Also, a larger (14 gauge) catheter was used in the expiratory channel to minimize the resistance, thus increasing the efficiency of the passive exhalation. A mix-

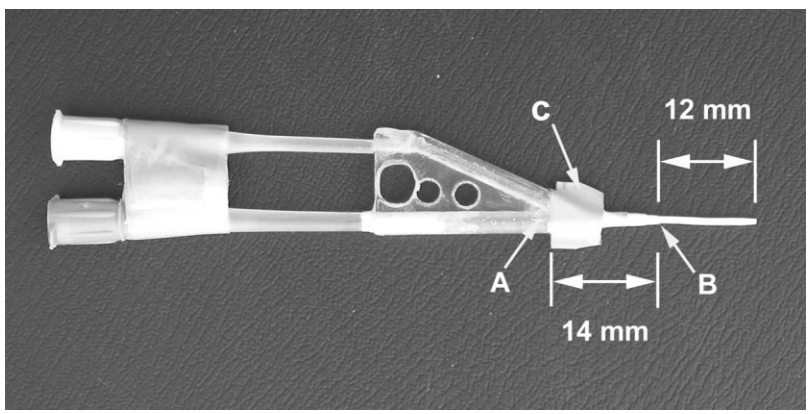

FIG. 2. Photograph of a Y-shape endotracheal (ET) tube is shown. The 16- and 14-gauge catheters were used to construct inspiratory and expiratory conduits, respectively. As depicted in Fig. 1, the length between point **a** and point **b** was measured (14 mm) from the two front teeth to the entrance of trachea of the mouse. The length of the convergent part of the ET tube was determined prior to intubation such that the tip was located in the manubrium (10–14 mm). Two wings (**c**) on the flank of the ET tube were used to secure the tube to the front incisors. This design minimizes the instrumental dead space.-

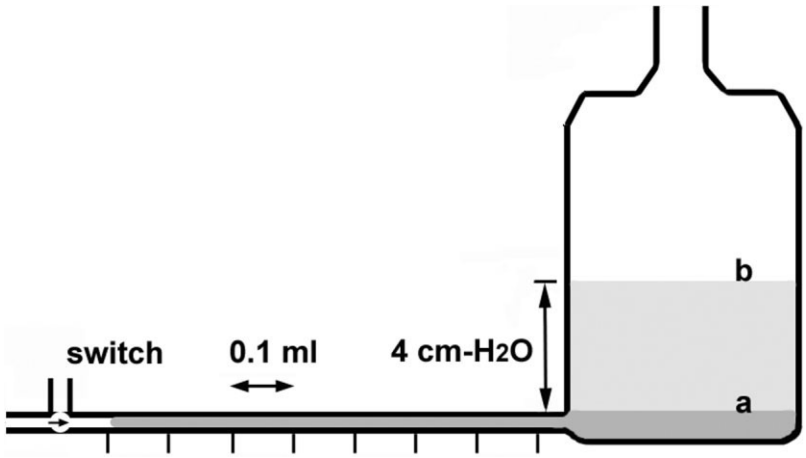

FIG. 3. Schematic of a spirometer used to calibrate the pneumotachometer at water level (**a**) and to verify the tidal volume (TV) at water level (**b**) is shown. The parts of the spirometer include a Teflon tube (1/4-inch diameter) and a jar with a side tubing connection. The volume of the tube is measured and marked at 0.1-mL increments. The displacement of the water in the tube during ventilation was used to calibrate the pneumotachometer. To simulate airway conditions in mice, 4 cm-H_2O was applied (b). As the water is oscillating in the tube, the wide-body jar is used so that the TV (~200 μL) cannot elevate the water level significantly. This device provides a simple method to verify tidal volume for small animals.

ture of 23% O_2 and 77% N_2 was supplied during normal breathing. During ^{3}He imaging, the mouse was ventilated with a mixture of 23% O_2 and 77% HP ^{3}He gas polarized to ~30%. While the mixture of O_2 can reduce the T_1 of the HP ^{3}He gas (20), the effects were minimal since all of the polarization was used in <100 msec after inhalation.

Anesthesia

Inducing anesthesia in mice presents challenging and often critical problems for MR in vivo lung imaging. Because of small body mass, mice can be easily overdosed. Inhalation anesthetics like halothane and isoflurane are effective for mice because of the rapid onset of and recovery from these drugs. Nevertheless, these volatile agents are known to inhibit hypoxia-induced vasoconstriction (21), a protective mechanism to redistribute blood circulation in the lung from poorly ventilated regions to sufficiently ventilated regions, which can alter lung images in asthmatic animal models. Also, inhibition of such a mechanism has been shown to associate with exacerbation of inflammatory responses in an injured lung (22), which often occurs in a mechanically ventilated lung. The combination of ketamine and diazepam has been shown in rats to produce less overall effect on pulmonary and cardiac function than other anesthetics, such as pentobarbital, fentanyl–droperidol combination, and ketamine–xylazine combination (23). This anesthetic regime provides an effective anesthesia for lung imaging studies in mice. Ketamine (56 mg/kg) and diazepam (2.8 mg/kg) were administered intraperitoneally to induce anesthesia.

Animal Preparation

A total of 40 male mice (C57BL/6, Charles River) weighing 20–25 g were used to develop animal support procedure (n = 31) and imaging protocol (n = 9). The animal protocol was approved by the Institutional Animal Care and Use Committee at Duke University.

The mouse was suspended in a supine position on a Plexiglas platform for oral intubation (24) allowing placement of the Y-shape ET tube (Fig. 3) into the trachea. The length of the catheter (22 gauge) was adjusted prior to insertion so that the tip of the catheter was positioned in the manubrium and the bifurcation of the tube was placed near the entrance of the trachea. To prevent air leaks due to positive pressure ventilation, an incision was made on the ventral neck skin, and blunt dissection was performed to expose the trachea for ligation (2-0 silk). The incised skin was then closed with a 3-0 suture (silk). To maintain anesthesia, the intraperitoneal space was cannulated (22-gauge, intravenous cannula, Sherwood Medical, Tullamore, Ireland) for bolus injections (0.02–0.04 mL) of ketamine (20 mg/mL) and diazepam (1 mg/mL). The injection was administered every 10–20 min to keep the heart rate under 400 beats/min, while the rectal temperature was maintained at approximately 37°C using warm air. The mouse (~25 g) was ventilated in a supine position at a rate of 105 breaths/min and TV of 0.2 mL. The tail vein was cannulated (26 gauge × 19 mm, Abbocath-T, Abbott Ireland, Sligo, Ireland) for infusion of intravascular contrast agent.

Imaging Procedure

All images were acquired on a 2.0-T horizontal-bore magnet (Oxford Instruments, Oxford, UK) with shielded gradients (180 mT/m), controlled by a Signa console (Epic 5X, General Electric Medical Systems, Milwaukee, WI). To acquire ^{1}H and ^{3}He images without repositioning the mouse, a 3.5-cm-diameter birdcage RF coil was constructed to operate with one mode resonant at 85.5 MHz for ^{1}H and the orthogonal mode resonant at 64.8 MHz for ^{3}He. Images were acquired using a slab-selective 3D anisotropic radial encoding sequence that was described previously (9,25). Briefly, a table of geodesic radial trajectories (views) was created in such a fashion that the end points of these views were uniformly distributed on the sphere defining the boundary of k-space being sampled. The sampling was made anisotropic along z by reducing the maximum distance covered along the k_z axis of Fourier space, resulting in a compression of boundary of Fourier coverage from a sphere into an oblate spheroid. The reconstruction method was based on a generalized gridding algorithm (26), in which the radial data were interpolated onto a Cartesian grid. The resolution of the images acquired by the radial sampling was defined by the view spacing at the edge of k-space. For these specific studies, a total of 32000 views were acquired for the ^{1}H images and 20480 views for

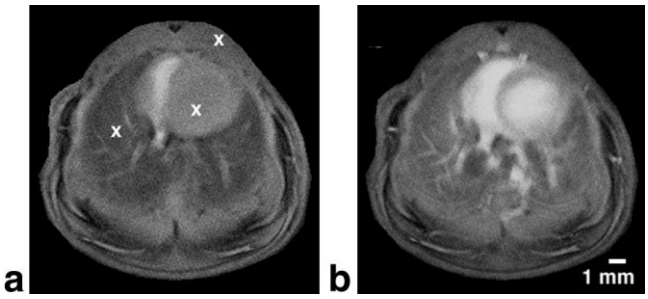

FIG. 4. Comparison of ^{1}H images prior-to (**a**) and after (**b**) the injection of the intravascular contrast agent. This macromolecular-based agent, G6–1B4M-Gd, does not leak through the vascular wall. The × marks indicate the regions of interest in the chest wall, left ventricle, and peripheral lung for signal-to-noise (SNR) analysis. The SNRs without contrast agent (a) are 4.8 in the chest wall, 5.9 in the left ventricle, and 3.5 in the peripheral lung, compared to 5.1, 11.7, and 6.6 after the administration of contrast agent (b). Contrast enhancement between the vasculature and the surrounding tissues is evident.

the ^{3}He images. More views were acquired for ^{1}H images due to low proton density in the lung. Data were gridded on 512 × 512 × 25 arrays resulting in a Nyquist-imposed resolution limit of 70 × 70 × 800 μm. Eight views were acquired during each 80-msec period of held breath (TR = 10 msec). Multiple breaths (4000 breaths for ^{1}H and 2560 breaths for ^{3}He) were used resulting in a scan time of 38 min for the ^{1}H images and 25 min for the ^{3}He images. The lower effective magnetization of the ^{1}H signal was offset by additional signal averaging; hence the difference in the number of views. Since we are encoding the free induction decay (FID), we report the "effective TE" of 1 msec, i.e., the time between the end of the excitation and the acquisition of the first point of the FID. The excitation angle α was 30° for the ^{1}H images. Since the ^{3}He magnetization undergoes a much wider range of excursion, α_n of the *n*th view of the eight samples acquired during each held breath was set according to the recursive relation $\alpha_{n-1} = arc\tan(\alpha_n)$ with $\alpha_n = 90°$, resulting in the most efficient use of polarization (27).

Contrast Agent

Macromolecular MRI contrast agent, G6–1B4M-Gd, was synthesized as previously described (28). The composition of the macromolecular agent G6–1B4M-Gd (C: 37.79%; H: 5.63%; N: 11.23%; S: 3.10%; Gd: 14.13%) was established by elemental analysis (Galbraith Laboratories, Knoxville, TN). The molecular weight (192 ± 1 kDa) and hydrodynamic radii (5.50 ± 0.04 nm) were determined by multiangle light scattering analysis (Wyatt Technology, Santa Barbara, CA). The macromolecular contrast agent remains in the blood vessels with a half-life of ~80 min (28,29). The long in vivo half-life provides a steady signal source for the extended (38 min) ^{1}H scan. Figure 4 shows a comparison of images prior to and after administration of the vascular contrast agent. We measured the signal-to-noise ratio (SNR), defined as the mean signal intensity in a given region of interest divided by the SD in the background. In Fig. 4, the SNR was increased by 129% in the left ventricle and 88% in the lung periphery with a 6% increase in the muscle of the chest wall after administration of the contrast agent. The percentage changes (mean ± error) in the SNR averaged overthree different animals were 81 ± 33, 43 ± 22, and −4 ± 5% in the left ventricle, the peripheral lung, and the chest wall, respectively. These results demonstrate that the Gd-labeled macromolecular contrast agent provides valuable contrast enhancement between vasculature and surrounding tissues in the lung.

^{3}He Polarization

A commercial polarizer (IGI.9600.He, Amersham Health, Durham, NC) employing spin exchange optical polarization (30) was used to polarize ~1200 mL of ^{3}He gas to 30–40% polarization in 8 hr.

Image Processing

^{1}H and ^{3}He images were combined (see Fig. 5). The 16-bit magnitude data were displayed in the "hot" colormap and the "gray" colormap using MATLAB software (The MathWorks, Natick, MA) to distinguish the ^{1}H and ^{3}He images, respectively. The display scale was mapped between 300 (background noise) and 80% of the maximum value in each respective image. Values outside the range were clamped to the first or last scale map color. For comparisons of the effect of the contrast agent on the ^{1}H images, the post-contrast images were displayed using the same display scale as the pre-contrast images. This normalization was done for display purposes only; the quantitative measurements of signal intensity were drawn from the original data that were not normalized.

RESULTS

Variations on the strategies were tested on a total of 40 animals. Images were acquired on a total of 9 animals to optimize the imaging parameters. Representative results from 3 different mice, acquired using the finalized animal procedure and imaging protocol described above, are shown. In our ventilation system, the compression index was 22 cm-H_2O/mL. To achieve TV of 8 mL/kg (0.2 mL for a 25-g mouse) under peak inspiratory pressure at 8 cm-H_2O, the ventilation was set to 0.56 mL. Stability of the mouse and success of the ventilation were determined by the absence of spontaneous breathing and stable heart rate. Through a combination of minimizing the dead space, accounting for gas compression in adjusting the TV, and careful maintenance of core body temperature at 37°C, we were able to maintain the anesthetized mouse in a stable state for more than 8 hr using the *I*/*E* ratio of 2/3 at the respiratory rate of 105 breath/min.

Figure 5 shows the selected slices from the combined 3D transverse pulmonary images of a live mouse, consisting of the vasculature-enhanced ^{1}H images (in color), and the airspace-enhanced ^{3}He images (in grayscale). Scan synchronous ventilation minimized the motion artifacts from breathing. Artifacts from cardiac motion were minimized

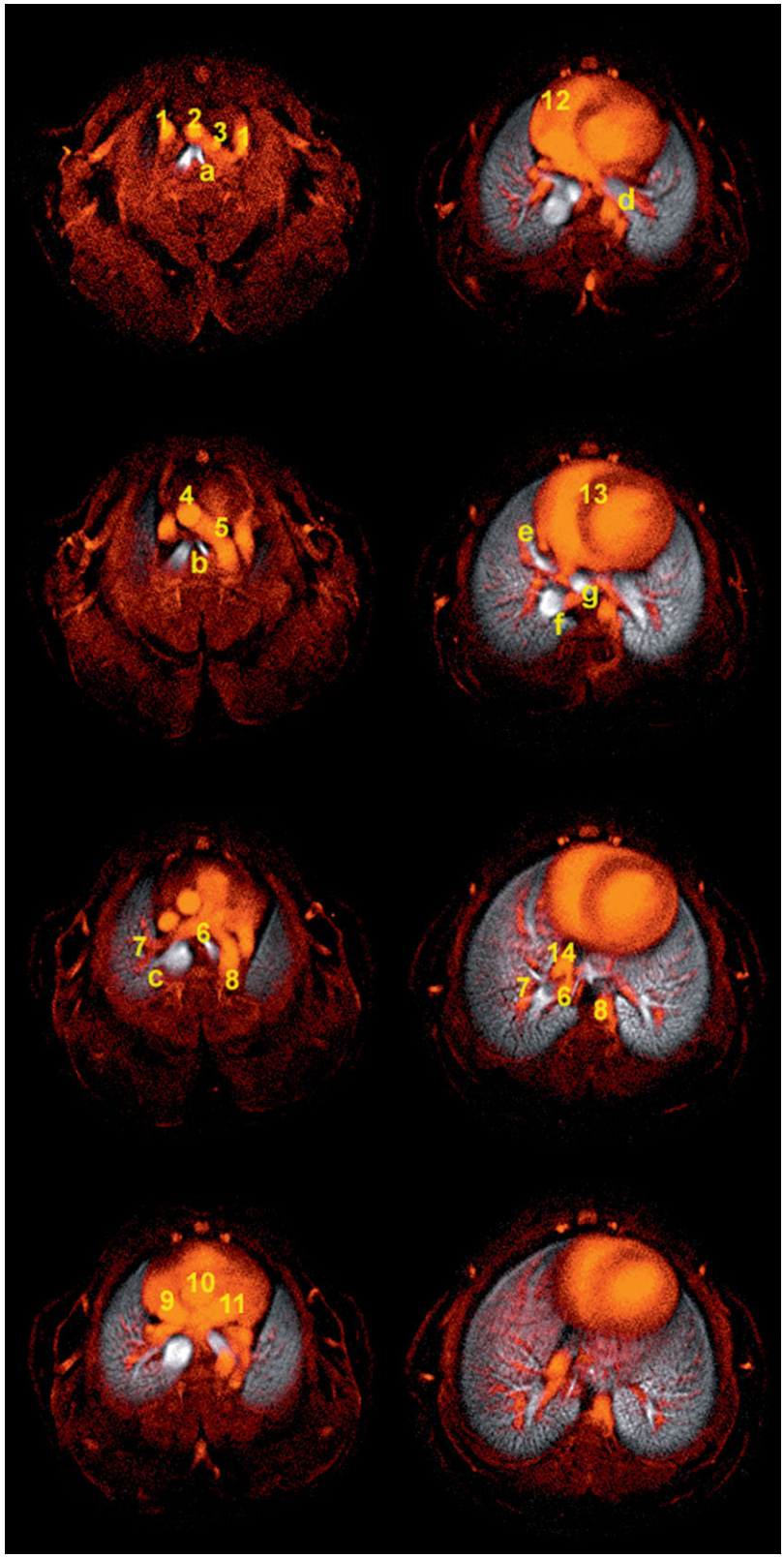

FIG. 5. Combined ^{1}H (color) and ^{3}He (gray) 3D transverse pulmonary images with anisotropic voxels ($70 \times 70 \times 800\ \mu m^3$) are shown. The transverse lung images of a superior-to-inferior sequence are displayed in the top-to-bottom and left-to-right order. The anatomic structures of heart and lung are demonstrated: (1) cranial vena cava; (2) innominate; (3) left common carotid; (4) ascending aorta; (5) arch of aorta; (6) pulmonary veins; (7) pulmonary arteries; (8) descending aorta; (9) right atrium; (10) left atrium; (11) left ventricle; (12) right ventricle; (13) intraventricular septum; (14) inferior vena cava; (a) carina; (b) bronchi; (c) branch to the right cranial lobe; (d) branch to the left lung; (e) branch to the right medial lobe; (f) branch to the right caudal lobe; (g) branch to the cardiac lobe.

by the signal averaging inherent in the 3D radial encoding method. Anatomic structures of the heart and lung at various slice selections were illustrated at microscopic resolution (voxels of 0.004 mm^3). The scaling factor we use for comparison of resolution in humans and mice is the voxel volume. The voxels shown in Fig. 5 are ~2500 times smaller than a typical pulmonary image in the human. A number of structures are labeled. Alignment of the ^{1}H and ^{3}He images can be appreciated by noting the alignment of vessels and airways in the coregistered images.

DISCUSSION AND CONCLUSIONS

Despite the small size of mice, the application of MR imaging to study structure and ventilation can be performed with proper care. In this article, we demonstrate coregistered images showing pulmonary structure and ventilation at microscopic resolution ($70 \times 70 \times 800$ μm^3 < 0.004 mm^3). Pulmonary vasculature (^1H) and ventilated airways (^3He) in the lung were acquired on the same live mouse during breath-hold with Gd-labeled dendrimer and HP ^3He gas using the 3D radial-sampling imaging technique. Other authors have demonstrated HP gas images (31) and ^1H images (11) in mice. The work here represents a reduction of voxel volume of nearly 78- and 5-times, respectively, and the first work to show coregistered ^1H and ^3He lung images. Such capabilities will clearly have application in phenotyping many of the newly developed genetic models of lung disease.

The increase in dead space due to instrumentation has been a major problem in imaging of small animals. At rest, mice (C57BL/6) breathe at ~164 breaths/min and ~73 μL/breath (32). Normally, a 22-gauge catheter is used to intubate a mouse. If the mouse is ventilated with such a small TV, the volume of the hub (>60 μL) of a 22-gauge catheter is large enough to exclude a significant portion of inspired fresh air from reaching the lung, resulting in hypoxemia. Levitt and his colleagues have demonstrated adequate ventilation in C57BL/6 mice (25 g) using a respiratory rate (RR) of 120 breath/min and a TV of 200–250 μL (33,34). Compared to spontaneous breathing at rest, twice the minute ventilation (TV × RR) required in the resting breathing was used to overcome the problems arising from the dead space. Under such a large TV, the *I*/*E* ratio must be small (<1/2) to allow completion of exhalation. In this study, we acquired images at a breath-hold, which is considered part of inhalation. A small *I*/*E* ratio in a breathing cycle causes unwanted increase in the scan time. For C57BL/6 mice, total lung capacity (TLC) measured at 30 cm-H_2O is ~1 mL and functional residual capacity measured at −5 cm-H_2O is 25% of the TLC (35,36). If the breathing rate was reduced (<80 breath/min) to increase the inhalation period, the large TV (>300 μL), which would be required to maintain adequate ventilation, could result in overextended airways. Separation of the inspired and expired airflow using a double-lumen ET tube could resolve the dead space problem (37). Nevertheless, the resistance for exhalation would increase by 16 times if the diameter of the tube for exhalation was reduced by half. A small *I*/*E* ratio would also be required with this approach. The Y-shape ET tube shown in Fig. 3 includes separate channels for inhalation and exhalation, allowing support of a mouse at 105 breath/min and tidal volume of 200 μL. This minute ventilation, less than what was used by Levitt and Mitzner (33), permits the use of a high *I*/*E* ratio to offer a longer acquisition window and shorter scan.

We used a slab-selective 3D anisotropic radial sampling sequence to acquire transverse images with in-plane resolution of 70×70 μm^2. Anisotropic sampling along *z* allows relatively short scan times (38 and 25 min for ^1H and ^3He imaging, respectively) with a trade-off of reduced resolution (800 μm) in the *z*-direction. We believe the resulting anisotropic voxels are a good compromise, particularly in the lung where the relative density of spins is such that the effects of volume averaging are less problematic than they might be in other more solid organs. Projection encoding further helps to minimize the consequences of cardiac motion, allowing an additional simplification in the acquisition method. While cardiac gating is clearly necessary for the most critical studies of the heart, the robustness of projection encoding to motion demonstrated for 2D encoding (38) is even more apparent with the increased averaging done for 3D encoding, particularly in the organ of interest—the lung (29).

As the inspired gas inflates the lung, pulmonary impedance imposes a back-pressure to compress the inspired gas within the inspiratory conduit. Consequently, a portion of the inspired gas does not reach the lung. To minimize loss of the HP ^3He gas due to gas compression, the pneumotachometer was only used for the normal ventilating mode to reduce the air volume of the ^3He conduit, as shown in Fig. 1.

While some of the methods reported here have been used previously in pulmonary studies of rats, extension to mice has required significant innovation. We believe that the techniques described in this article will serve as the groundwork for the application of MR microscopy to the rapidly growing studies of transgenic/knockout mice where advanced imaging methods are needed.

ACKNOWLEDGMENTS

The authors are grateful to Ted Wheeler and Gary Cofer for technical assistance. We thank Dr. Laurence Hedlund for useful discussions and Sally Zimney for assistance in preparation of the manuscript. This work was performed at the Duke Center for In Vivo Microscopy.

REFERENCES

1. D'Armiento J, Dalal SS, Okada Y, Berg RA, Chada K. Collagenase expression in the lungs of transgenic mice causes pulmonary emphysema. Cell 1992;71:955–961.
2. Korfhagen TR, Swantz RJ, Wert SE, McCarty JM, Kerlakian CB, Glasser SW, Whitsett JA. Respiratory epithelial cell expression of human transforming growth factor-alpha induces lung fibrosis in transgenic mice. J Clin Invest 1994;93:1691–1699.
3. Nagase T, Kurihara H, Kurihara Y, Aoki T, Fukuchi Y, Yazaki Y, Ouchi Y. Airway hyperresponsiveness to methacholine in mutant mice deficient in endothelin-1. Am J Respir Crit Care Med 1998;157:560–564.
4. Finotto S, Neurath MF, Glickman JN, Qin S, Lehr HA, Green FH, Ackerman K, Haley K, Galle PR, Szabo SJ, Drazen JM, De Sanctis GT, Glimcher LH. Development of spontaneous airway changes consistent with human asthma in mice lacking T-bet.[comment]. Science 2002; 295:336–338.
5. Hedlund LW, Johnson GA, Karis JP, Effmann EL. MR microscopy of the rat thorax. J Comput Assist Tomogr 1986;10:948–952.
6. Gewalt SL, Glover GH, Hedlund LW, Cofer GP, MacFall JR, Johnson GA. MR microscopy of the rat lung using projection reconstruction. Magn Reson Med 1993;29:99–106.
7. Kuethe DO, Caprihan A, Fukushima E, Waggoner RA. Imaging lungs using inert fluorinated gases. Magn Reson Med 1998;39:85–88.
8. Cremillieux Y, Berthezene Y, Humblot H, Viallon M, Canet E, Bourgeois M, Albert T, Heil W, Briguet A. A combined ^1H perfusion/^3He ventilation NMR study in rat lungs. Magn Reson Med 1999;41:645–648.
9. Johnson GA, Cofer GP, Hedlund LW, Maronpot RR, Suddarth SA. Registered ^1H and ^3He magnetic resonance microscopy images of the lung. Magn Reson Med 2001;45:365–370.
10. Kuethe DO, Behr VC, Begay S. Volume of rat lungs measured throughout the respiratory cycle using ^{19}F NMR of the inert gas SF6. Magn Reson Med 2002;48:547–549.

11. Garbow JR, Zhang Z, You M. Detection of primary lung tumors in rodents by magnetic resonance imaging. Cancer Res 2004;64:2740–2742.
12. Hedlund LW, Johnson GA. Mechanical ventilation for imaging the small animal lung. ILAR J 2002;43:159–174.
13. Shattuck MD, Gewalt SL, Glover GH, Hedlund LW, Johnson GA. MR microimaging of the lung using volume projection encoding. Magn Reson Med 1997;38:938–942.
14. Middleton H, Black R, Saam B, Cates G, Cofer G, Guenther B, Happer W, Hedlund L, Johnson G, Juvan K, Swartz J. MR imaging with hyperpolarized He-3 gas. Magn Reson Med 1995;33:271–275.
15. Viallon M, Cofer GP, Suddarth SA, Möller H, Chen XJ, Chawla MS, Hedlund LW, Crémillieux Y, Johnson GA. Functional MR microscopy of the lung with hyperpolarized ^{3}He. Magn Reson Med 1999;41:787–792.
16. Deninger AJ, Mansson S, Petersson JS, Pettersson G, Magnusson P, Svensson J, Fridlund B, Hansson G, Erjefeldt I, Wollmer P, Golman K. Quantitative measurement of regional lung ventilation using ^{3}He MRI. Magn Reson Med 2002;48:223–232.
17. Chen BT, Brau ACS, Johnson GA. Measurement of regional lung function in rats using hyperpolarized ^{3}Helium dynamic MRI. Magn Reson Med 2003;49:78–88.
18. Gomes RF, Shen X, Ramchandani R, Tepper RS, Bates JH. Comparative respiratory system mechanics in rodents. J Appl Physiol 2000;89:908–916.
19. Schuessler TF, Bates JH. A computer-controlled research ventilator for small animals: design and evaluation. IEEE Trans Biomed Eng 1995;42:860–866.
20. Saam B, Happer W, Middleton H. Nuclear relaxation of ^{3}He in the presence of O_2. Phys Rev A 1995;52:862–865.
21. Bjertnaes LJ. Hypoxia-induced vasoconstriction in isolated perfused lungs exposed to injectable or inhalation anesthetics. Acta Anaesthesiol Scand 1977;21:133–147.
22. Nader-Djalal N, Knight PR, Bacon MF, Tait AR, Kennedy TP, Johnson KJ. Alterations in the course of acid-induced lung injury in rats after general anesthesia: volatile anesthetics versus ketamine. Anaesth Analg 1998;86:141–146.
23. Wixson SK, White WJ, Hughes HC, Jr., Lang CM, Marshall WK. The effects of pentobarbital, fentanyl-droperidol, ketamine-xylazine and ketamine-diazepam on arterial blood pH, blood gases, mean arterial blood pressure and heart rate in adult male rats. Lab Anim Sci 1987;37:736–742.
24. Brown RH, Walters DM, Greenberg RS, Mitzner W. A method of endotracheal intubation and pulmonary functional assessment for repeated studies in mice. J Appl Physiol 1999;87:2362–2365.
25. Kust MP, Shattuck MD, Glover GH, Johnson GA. Anisotropic methods for three-dimensional projection magnetic resonance imaging. 1997; Vancouver, BC. p 1996.
26. Jackson JI, C.H. M, Nishimura DG, A: M. Selection of a convolution function for Fourier inversion using gridding. IEEE Trans Med Imag 1991;10:473–478.
27. Johnson GA, Cates G, Chen XJ, Cofer GP, Driehuys B, Happer W, Hedlund LW, Saam B, Shattuck MD, Swartz J. Dynamics of magnetization in hyperpolarized gas MRI of the lung. Magn Reson Med 1997;38:66–71.
28. Yordanov AT, Kobayashi H, English SJ, Reijnders K, Milenic D, Krishna MC, Mitchell JB, Brechbiel MW. Gadolinium-labeled dendrimers as biometric nanoprobes to detect vascular permeability. J Mater Chem 2003;13:1523–1525.
29. Brau ACS, Hedlund LW, Johnson GA. Cine magnetic resonance microscopy of the rat heart using cardiorespiratory-synchronous projection reconstruction imaging. J Magn Reson Imaging 2004;20:31–38.
30. Happer W, Miron E, Schaefer S, Schreiber D, Wijngaarden W, Zeng X. Polarization of the nuclear spins of noble-gas atoms by spin exchange with optically pumped alkali-metal atoms. Phys Rev A 1984;29:3092–3110.
31. Wagshul M, Button TM, Li HF, Liang Z, Springer CS, Zhong K, Wisnia A. In vivo MR imaging and spectroscopy using hyperpolarized 129Xe. Magn Reson Med 1996;36:183–191.
32. Han F, Subramanian S, Dick TE, Dreshaj IA, Strohl KP. Ventilatory behavior after hypoxia in C57BL/6J and A/J mice. J Appl Physiol 2001;91:1962–1970.
33. Levitt RC, Mitzner W. Expression of airway hyperreactivity to acetylcholine as a simple autosomal recessive trait in mice. FASEB J 1988;2:2605–2608.
34. Henderson WR, Jr., Lewis DB, Albert RK, Zhang Y, Lamm WJ, Chiang GK, Jones F, Eriksen P, Tien YT, Jonas M, Chi EY. The importance of leukotrienes in airway inflammation in a mouse model of asthma. J Exp Med 1996;184:1483–1494.
35. Tankersley CG, Rabold R, Mitzner W. Differential lung mechanics are genetically determined in inbred murine strains. J Appl Physiol 1999;86:1764–1769.
36. Lai YL, Chou H. Respiratory mechanics and maximal expiratory flow in the anesthetized mouse. J Appl Physiol 2000;88:939–943.
37. Chen BT, Yeates DB. Differentiation of ion-associated and osmotically driven water transport in canine airways. Am J Respir Crit Care Med 2000;162:1715–1722.
38. Glover G, Pauly J. Projection reconstruction techniques for reduction of motion effects in MRI. Magn Reson Med 1992;28:275–289.